Geophys. Astrophys. Fluid Dynamics, Vol. 88, pp. 1–30
Reprints available directly from the publisher
Photocopying permitted by license only

ON THE INFLUENCE OF AN ISOLATED SUBMERGED OBSTACLE ON A BAROTROPIC TIDAL FLOW

M. A. SOKOLOVSKIY [a], V. N. ZYRYANOV [a]
and P. A. DAVIES [b,*]

[a] *Institute of Water Problems, Russian Academy of Sciences, Novaya Basmannaya 10, 107078 Moscow, Russia;*
[b] *Department of Civil Engineering, The University, Dundee DD1 4HN, UK*

(Received 29 September 1997; In final form 23 December 1997)

The influence of an isolated submerged obstacle on the dynamics of a material particle is studied within the limits of a barotropic, quasi-geostrophic model of oceanic *f*-plane flow, for cases in which the incident flow has both steady and tidal components of velocity. Two kinds of motion are shown to occur, namely (i) the particle performs quasi-periodic oscillations in the vicinity of the obstacle or (ii) the particle acquires an infinite character (*i.e.*, the particle leaving the vicinity of the obstacle is irrevocably advected downstream by the background flow). Sufficient conditions are obtained for the existence of both classes of motion. Conditions for domain alternation of the finite and infinite solutions have been derived numerically for different external parameters (*e.g.*, the kinematic characteristics of the flow field and the height of topography). Using the Contour Dynamics Method, results are presented to show how the predicted motions of individual particles can be extended to predict the behaviour of finite water volumes in general and particle admixture patches in particular.

Keywords: Barotropic tidal flow; submerged obstacle; quasi-geostrophic; oceanic *f*-plane

1. INTRODUCTION

Though a large number of investigations have dealt with the modelling of the influence of bottom relief on steady oceanic currents (see the reviews by Kozlov, 1983; Zyryanov, 1985, 1995; Roden, 1987; Thompson, 1990 and Baines, 1993), studies examining the effects of

*Corresponding author.

submarine topographic features are comparatively rare for cases in which the incident currents vary periodically with time. Of these, Verron (1986) has presented the results of numerical modelling investigations on the formation and drift of topographically-trapped and advected vortices in the vicinity of a small topographic feature exposed to a unidirectional, time-varying incident flow $u(t)$ of the form $u = U(1-\cos \omega t)$. Likewise, the dynamics of a weakly-periodic, zonal flow $u = U(1-\varepsilon \cos \omega t)$, $\varepsilon \ll 1$ over an infinite crest has been discussed by Kozlov and Sokolovskiy (1981). Chen and Beardsley (1995); Chen *et al.* (1995); Beckmann and Haidvogel (1993) carried out numerical modelling studies to determine the behaviour of a purely oscillating flow $u = U \cos \omega t$ when interacting with an isolated obstacle of finite height and, more recently, Goldner and Chapman (1997) have studied the induced motions caused by interactions of steady and tidal background currents with a tall seamount. Laboratory studies (Boyer *et al.*, 1991; Zhang and Boyer, 1993; Perera *et al.*, 1995) of topographic interactions of oscillating flows are related closely with the above investigations.

Most previous studies have examined either pulsating or purely reversing flows, with oscillating currents having been poorly investigated thus far; in particular, currents changing their direction and developing against the background of a constant component require further study. As experimental observations show, currents of this type are often the most characteristic for the ocean. For example, current observations (Eriksen, 1991) in the area of Fieberling guyot show that between 39% and 48% of total kinetic energy is contained in the tidal movements. Brink (1995) has demonstrated that for Fieberling, the tidal forcing of the flow can lead to significant selective amplification of tidal constituents of the current record. Likewise, detailed investigations by Smith *et al.* (1989) have shown in the framework of the TOPO programme that daily oscillations of velocity with amplitudes of $0.2-0.4\,\mathrm{m\,s^{-1}}$ are found on background constant flows with velocities of about $0.1\,\mathrm{m\,s^{-1}}$. Other field measurements (Gibson *et al.*, 1994; Roden, 1991) give velocities of the tidal and constant components of the flow of $0.48\,\mathrm{m\,s^{-1}}$ and $0.01\,\mathrm{m\,s^{-1}}$ respectively, while analyses of current measurements in the Atlantic ocean in the area of the Ampere seamount (Monin *et al.*, 1989) show the oscillating component to be approximately three times greater than the background.

It is known that oceanic regions with pronounced topographic irregularities may coincide with areas of high concentrations of fish and other marine species, as a result of the heightened presence there of mineral salts, phyto- and zoo-plankton and other elements of the trophic chain. These elements can be regarded as particles or patches of passive admixture, their dynamics being amenable to study, as here, with Lagrangian methods. A similar approach applied to the study of the distribution of nutrient substances over a chain of underwater banks in the region of Vancouver Island was used in Foreman *et al.* (1992). Tracer methods have also been widely used for studying chaotic advection (see for example, Ziemniak *et al.*, 1994) and in tidal flows (Beerens *et al.*, 1994).

The present study is based upon the above-mentioned Lagrangian approach and considers the influence in a rotating fluid of an isolated underwater obstacle of small height on the current flowing around it. In general, this current has a periodic component with a non-degenerated ellipse oriented arbitrarily with respect to the direction of the general stationary transport. Attention is directed specifically on determining approximate criteria for the existence of quasi-periodic regimes of flow.

2. FORMULATION OF THE PROBLEM

The study is limited to cases in which the quasi-geostrophic approximation is valid in a uniform, f-plane rotating ocean with a topographic disturbance siginificantly smaller than the mean depth H. Sufficiently far from the topographic feature of height h, the components $(\bar{u}, \bar{v})$ of the current velocity along axes of a rectangular coordinate system (x, y, z) rotating uniformly with angular velocity $(0, 0, f/2)$ are specified by the relations

$$\bar{u} = U_0 + U \cos \omega t, \tag{1}$$

$$\bar{v} = V_0 + V \sin \omega t, \tag{2}$$

where U_0 and V_0 are the x- and y-components of the constant background velocity and U and V are corresponding amplitudes of

periodic perturbations with frequency ω. For oceanic cases, using a typical velocity scale of $V^* = 0.2\,\mathrm{m\,s^{-1}}$ and with $f = 1.4\times10^{-4}\,\mathrm{s^{-1}}$ as Coriolis parameter and $T = 12$ hour $= 4.32\times10^4$ s as time, then the horizontal scale L^* of the topographic disturbance will be $L^* \sim 8.6$ km and the non-dimensional wave frequency corresponding to the daily tidal oscillations, $\omega = \pi$. In consequence, the value of the Rossby number $Ro = V^*/fL^* = \mathrm{O}(10^{-1})$, confirming that the quasi-geostrophic approximation is valid for such cases. The possibility of applying the quasi-geostrophic approximation to tidal, oceanic flows has been substantiated rigorously in Zyryanov (1995).

A tidal current of the form (1)–(2) flows around a submerged topographic feature of amplitude h, the shape of which is taken to be (in non-dimensional coordinates) an upright circular cylinder of unit radius. Then, the resulting background current velocity components (u, v) that satisfy the condition of potential vorticity conservation will be determined by the superposition of this current and the topographic vortex (Kozlov, 1983; Zyryanov, 1985, 1995) induced by the disturbance

$$u = \bar{u} + (\sigma/2)\, y\, G(r), \tag{3}$$

$$v = \bar{v} - (\sigma/2)\, y\, G(r), \tag{4}$$

$$G(r) = \begin{cases} 1, & r \le 1, \\ 1/r^2, & r > 1, \end{cases} \qquad r^2 = x^2 + y^2, \tag{5}$$

where $\sigma = h/H(Ro) = \mathrm{O}(1)$ is the topographic parameter (taking positive and negative values for elevated or depressed topographic features respectively). For the typical oceanic values cited above and with $H \sim 4$ km, a value of $\sigma = 1$ corresponds to a positive topographic feature of height 640 m. The relation $\sigma = \mathrm{O}(1)$ sets a formal "smallness" criterion for bottom disturbances, namely $h \sim H(Ro)$.

The Eqs. (3)–(4) can be written in the form of ordinary differential equations for the movement of a material point as

$$dx/dt = U_0 + U\cos\omega t + (\sigma/2)\, y\, G(r), \tag{6}$$

$$dy/dt = V_0 + V\sin\omega t - (\sigma/2)\, x\, G(r), \tag{7}$$

$$t = t_0; \quad x = x_0; \quad y = y_0. \tag{8}$$

It is possible to consider the system (6)–(8) as a mathematical model for the dynamics of a point vortex having arbitrary intensity, because the self-influence in case of a single discrete vortex is absent.

It is of interest to consider the simplest particular case, where there is no topographic disturbance ($\sigma = 0$). The system (6)–(8) gives solutions

$$x = x_0 + U_0 t + (U/\omega) \sin \omega t, \tag{9}$$

$$y = y_0 + V_0 t + (V/\omega)(1 - \cos \omega t), \tag{10}$$

showing that a fluid particle performing loop-shaped oscillations is drifted in the direction of the mean flow. At $U_0 = V_0 = 0$ every particle moves along the elliptic trajectory

$$[(x - x_0)/(U/\omega)]^2 + \{[(y - y_0) - (V/\omega)]/[V/\omega]\}^2 = 1 \tag{11}$$

around the individual centre $[x_0, (y_0 + (V/\omega))]$ in the cyclonic (anti-cyclonic) direction at $UV > 0$, $(UV < 0)$.

In the general case, interest will be directed at fluid particle movements described by the flow of the form (1)–(2) that is evolving against the background of an axially-symmetric gyre induced by the topography. The direction of the movement is anticyclonic over a positive obstacle and cyclonic over a depression.

2.1. Topological Peculiarities of the Background Field

The external field (3)–(4) can have two singular points where the velocity vector is zero-the elliptic point (x_e, y_e) within the limits of the unit circle and the hyperbolic point (x_h, y_h) outside this circle-with coordinates

$$\begin{aligned} (x_e, y_e) &= (2v/\sigma, -2u/\sigma), \\ (x_h, y_h) &= [\sigma v/2(u^2 + v^2), (-\sigma u)/2(u^2 + v^2)]. \end{aligned} \tag{12}$$

In the second singular point there occurs the self-crossing of the separatrix surrounding the area of topographic trapping. According to

(1)–(2), coordinates $x_{e,h}$, $y_{e,h}$ are explicit functions of time. It follows from (12) that (i) if

$$U_0^2 + V_0^2 + [\max(|U|, |V|)]^2 + 2[(U U_0)^2 + (V V_0)^2]^{1/2} \leq \sigma^2/4 \tag{13}$$

then singular points exist for any t, and (ii) if

$$U_0^2 + V_0^2 + [\min(|U|, |V|)]^2 - 2[(U U_0)^2 + (V V_0)^2]^{1/2} > \sigma^2/4 \tag{14}$$

there are no such points. Denoting the topographic parameter limit values (*i.e.*, those that satisfy the equality in (13) and (14)) as $\sigma_{\max}$ and $\sigma_{\min}$ at fixed kinematic characteristics of the background field, the velocity vector at

$$|\sigma_{\min}| < |\sigma| < |\sigma_{\max}| \tag{15}$$

will clearly become zero in points $(x_{e,h}, y_{e,h})$ that appear only in some time interval of every tidal period.

Figure 1 shows examples of relations $x_{e,h}(t)$, $y_{e,h}(t)$ and $y_{e,h}(x_{e,h})$, for cases (13) and (15). For the selected values of velocity, $\sigma_{\max} = 2.97$, $\sigma_{\min} = 0.36$. Clearly, (i) condition (13) is fulfilled in case (a) and (ii) condition (15) is fulfilled in cases (b) and (c). (Note that here, and in all other figures unless specified otherwise, the dashed circular line of unit radius represents the boundary of the underwater obstacle).

In cases where conditions (13)–(15) are satisfied, the following properties are anticipated:

(a) all fluid particles localised inside the area bounded by the evolving separatrix should remain in the vicinity of the topography;
(b) all particles (including those passing over the top of the obstacle) are advected in the direction of the mean flow;
(c) there may exist areas of trapping, partially ventilated by new fluid particles.

In case (c), because of the initial conditions (8), the selected individual particle should either remain as long as possible in the vicinity of the topography or, after finishing the initial stage of quasi-

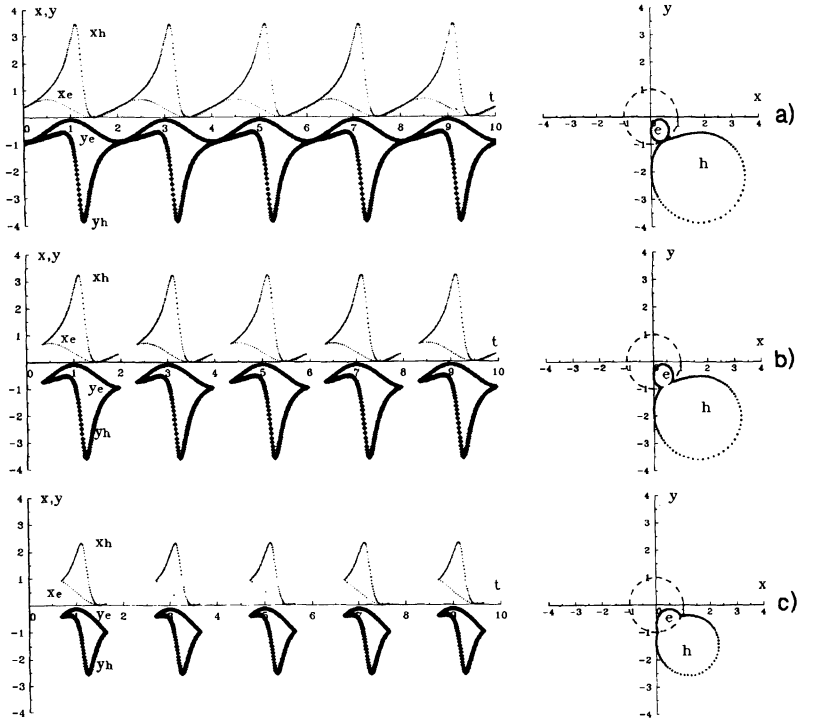

FIGURE 1 Plots of (i) $x_{e,h}$ (normal) and $y_{e,h}$ (bold) versus time t and (ii) $y_{e,h}$ versus $x_{e,h}$, at $\omega=\pi$, $U_0=0.75$, $V_0=0.5$, $U=0.6$, $V=0.5$ and $\sigma=$(a) 3, (b) 2.8, (c) 2.0. Designations "e" and "h" denote trajectories of elliptic and hyperbolic specific points respectively.

periodic localized movements and being found outside the newly-formed separatrix, be advected downstream.

2.2. Dynamics of a Fluid Particle in the Vicinity of a Submerged Topographic Feature

2.2.1. Particle Over the Topography ($r \leq 1$)

If the particle does not leave the limits of the unit circle during its movement (*i.e.*, it remains over the topographic feature), the system (6)–(8) is linear and has an analytical solution

$$x = a\cos(\sigma t/2) + b\sin(\sigma t/2) + [A\sin\omega t + B\sin(\sigma t/2)]/C \equiv x_S + x_T, \tag{16}$$

$$y = b\cos(\sigma t/2) - a\sin(\sigma t/2) + B[\cos\omega t - \cos(\sigma t/2)]/C \equiv y_S + y_T. \tag{17}$$

Here, $a = x_0 - (2V_0/\sigma)$, $b = y_0 + (2U_0/\sigma)$, $A = U\omega - (V\sigma/2)$, $B = V\omega - (U\sigma/2)$, $C = \omega^2 - (\sigma^2/4)$ and subscripts S and T correspond to terms arising due to stationary and oscillating components respectively of the external current. The requirement for the particle to remain over the topography imposes restrictions on the external parameter combinations

$$\begin{aligned} &r_0 + (4W_0/\sigma) + (2B/C) \le 1, && A^2 \le B^2, \\ &r_0 + (4W_0/\sigma) + [(A+B)/C] \le 1, && A^2 > B^2, \end{aligned} \tag{18}$$

where $r_0 = (x_0^2 + y_0^2)^{1/2}$ and $W_0 = (U_0^2 + V_0^2)^{1/2}$. Note that the expressions (18) are only sufficient conditions for fulfilling the inequality $r \le 1$. It is obvious that at the given velocities of the background current, the relations (18) represent more rigid constraints on the topographic disturbance than the conditions (13).

For cases of stationary background currents ($U = V = 0$), conditions (18) and the solutions (16)–(17) determine a set of circular trajectories of the type

$$\begin{aligned} &[x - (2V_0/\sigma)]^2 + [y + (2U_0/\sigma)]^2 \\ &\quad = r_0^2 + (4W_0^2/\sigma^2) - (4r_0 W_0/|\sigma|)\cos(\beta - \alpha), \end{aligned} \tag{19}$$

where $\cos\alpha = V_0/W_0$, $\sin\alpha = -U_0/W_0$, and the angle β is defined by $\cos\beta = x_0/r_0$; $\sin\beta = y_0/r_0$. Thus, if a fluid particle having been inside a kinematically-stationary flow does not leave the limits of the topographic feature during its motion, it can move only along some circular orbit within the Taylor column (Ingersoll, 1969). The external boundary of this column coincides with the limiting location of the circle [see Eq. (19)] that touches the boundary of the feature.

As can be seen from (16)–(17), the tidal part of the current (x_T, y_T) represents a superposition of oscillations (modulated along the y-axis) with frequencies ω and $\sigma/2$. This component of the solution has resonance at $C = 0$ ($\omega = \pm\sigma/2$), when there are no solutions bounded uniformly in time, as $U \neq V$ in the area $r \le 1$.

If $U=V$ (when, clearly, $A=B$ and the tidal ellipse of the external field will have the shape of a circle), periodic modulated oscillations take place along both axes:

$$x_T=\{2U/[(\omega)+(\sigma/2)]\}\sin\{[(\omega)+(\sigma/2)][t/2]\}\cos\{[(\omega)-(\sigma/2)][t/2]\}, \tag{20}$$

$$y_T=\{-2U/[(\omega)+(\sigma/2)]\}\sin\{[(\omega)+(\sigma/2)][t/2]\}\sin\{[(\omega)-(\sigma/2)][t/2]\}, \tag{21}$$

and the singularity is observed only at $\omega=-\sigma/2$, when the tidal and topographic components of the external field induce rotation of the same sign. Now, at $\omega=\sigma/2$ the solutions (16)–(17) take the simplest form

$$x-(2V_0/\sigma)=a\cos\omega t+c\sin\omega t, \tag{22}$$

$$y+(2U_0/\sigma)=b\cos\omega t-a\sin\omega t, \tag{23}$$

where $c=b+(U/\omega)$. It is easy to show that the relations (22)–(23) define a family of ellipses with centres at the point $(2V_0/\sigma, -2U_0/\sigma)$, similar to the circles (19) and with semi-axes A_1, A_2:

$$A_{1,2}=(a^2+bc)/[(a^2+b^2)\cos^2\gamma \pm 2a(c-b)\sin\gamma\cos\gamma+(a^2+c^2)\sin^2\gamma]^{\frac{1}{2}}. \tag{24}$$

The first of these semi-axes makes an angle γ with the x-axis, such that $\tan 2\gamma=-2a/(b+c)$.

The solutions (16)–(17) has a periodic structure when quantities ω and $\sigma/2$ are commensurable. Figure 2 demonstrates examples of periodic trajectories for the case $\omega=n(\sigma/2)$, for integer values of n. The amplitudes U, V of tidal components of the external flow were calculated from the condition of strict equality in (18). The trajectory of the particle that started its motion at the origin (0, 0) and moves with the tidal flow, having a circular ellipse, is given in Figure 2a. Figure 2b shows a similar plot for the particle with initial coordinates (0, 0.5). Further, Figure 2c corresponds to the tidal ellipse of the background field being stretched by a factor 2 along the x axis and Figure 2d represents the stationary x-velocity component to be added

to the background field. In Figures 2(c, d) at $n=1$, evidently $V=0$, as in this (resonant) case finite solutions exist only when the periodic component of the external field is absent. Clearly, however, frequencies are higher than in the tidal oscillation frequencies in this case.

It is possible to note the case $a=0$ of purely periodic motions that take place for any relationship between ω and σ. For this case, the trajectories of the particles coincide with the curves of the form

$$\{[x-(2V_0/\sigma)-D\sin(\sigma t/2)]/E\}^2 + \{[y+(2U_0/\sigma)-D\cos(\sigma t/2)]/J\}^2 = 1, \tag{25}$$

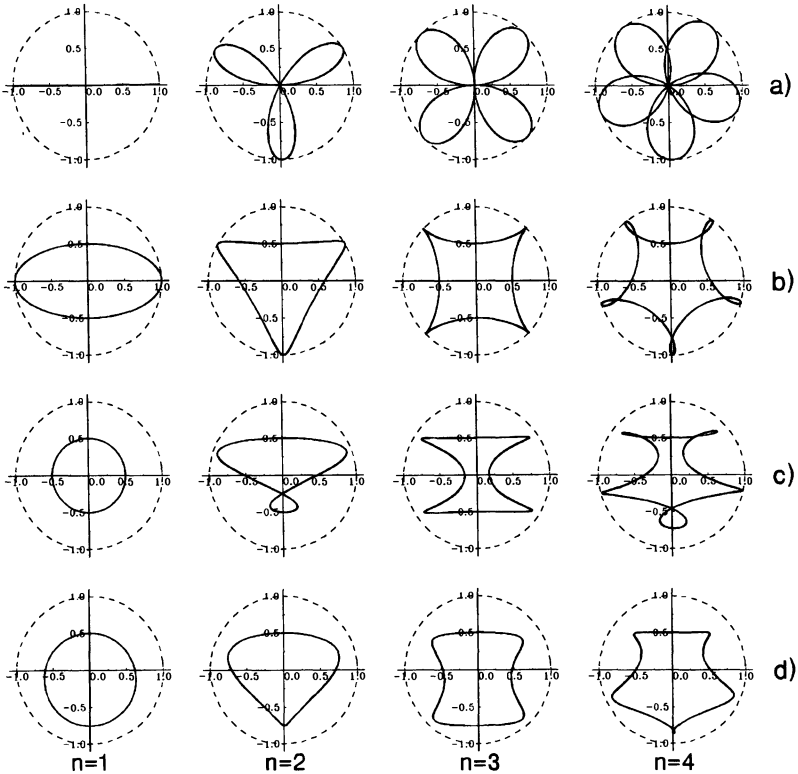

FIGURE 2 Trajectories of a liquid particle at $\sigma=4$, $\omega=n\sigma/2$, $x_0=0$ and $[y_0: U_0: V_0: U/V]$ = (a) [0:0:0:1], (b) [0.5:0:0:1], (c) [0.5:0:0:2], (d) [0.5:0.25:0:2].

where $D=b+(B/C)$, $E=A/C$ and $J=B/C$. Such trajectories become ellipses at $D=0$.

Figure 3 shows circular (a) and elliptical (b) fluid particle trajectories; they are identical but have been obtained under different external parameters. So the left column of this figure shows the curves over the obstacle along which the particle moves in a stationary flow [according to (19)]–(1a) and in the flow with tidal component [according to (25)]–(1b). The right column gives analogous trajectories that are followed by the particle [according to (11)] in the tidal flow over the flat bottom. Here, the centres of the circles and ellipses are located respectively at coordinates (0.108; −0.250) and (0.108; −0.091), with the radius of the circles being 0.704 and x- and y-semi-axes of the ellipses having values of 0.705 and 0.864 respectively.

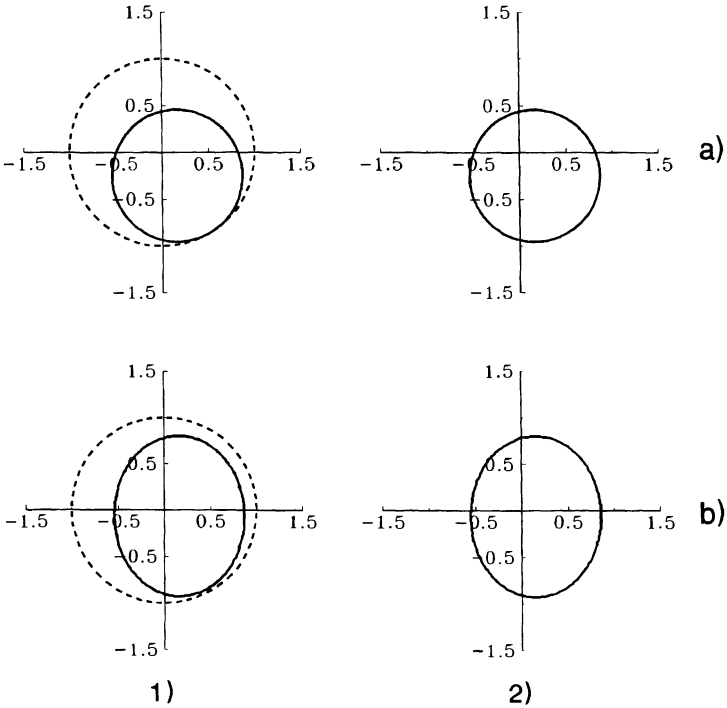

FIGURE 3 Trajectories of a fluid particle $\omega=\pi$, $x_0=0.108$, $y_0=-0.954$ for $[\sigma:U_0:V_0:U:V]$ = (1a) [4:0.5:0.216:0:0], (1b) [4:0.182:0.216:3.941:4.121], (2a) [0:0:0:2.212:2.212] and (2b) [0:0:0:2.215:2.713].

This example demonstrates the need for information not only on the velocities of the flow but also on the bottom topography, when interpreting results of tracer observations.

The above examples illustrate only some of the set of possible solutions. In the more complicated case of two arbitrary independent frequencies, the resulting trajectories have more complex configurations. As it will be seen below in Figure 9, they can have either a relatively ordered or very complicated structure. In the latter case, trajectories essentially fill an area inside the unit circle.

2.2.2. *A Particle in the Vicinity of the Topographic Feature*

When $r > 1$, an analytical solution of the system (6)–(8) is not possible because of non-linearity. So, in the general case, use is made of a numerical algorithm that admits the transition from one form of the right-hand side expressions in (6)–(7) to another when a fluid particle crosses the boundary $r = 1$. In the present case, a Runge-Kutta method of second order of accuracy was used with a time step of $\Delta t = 0.01$.

It has been established that at $C = 0$, arbitrary values of U_0, V_0 and $U \neq V$ [and in circumstances where the conditions (18) are not already satisfied], the particle inevitably leave the limits of the unit circle (see Fig. 4), where the solution (9)–(10) is no longer valid. This result is a demonstration of the "resonance" properties of the system. In all cases given in the figure, the conditions (15) are fulfilled and the particle trajectories remain localised in the vicinity of the topography (at least over the calculation time interval of 500 dimensionless units, with a time scale taken to be 12 hours). All numerical experiments of this series have been fulfilled when the external field had tidal ellipses stretched in the zonal direction ($U/V = 1.6$). The following cases were examined: (a) steady state component of the current absent; (b) current has x-component only and (c) current has y-component only. For each case, the initial location of the fluid particle at $x_0 = 0$ is indicated in the bottom part of the figure. The different states of regulation of various trajectories, noted at the end of Section 2.2.1, are noticeable. Some concerns about this matter are considered below in Section 3. Note the qualitative resemblance of the trajectories given

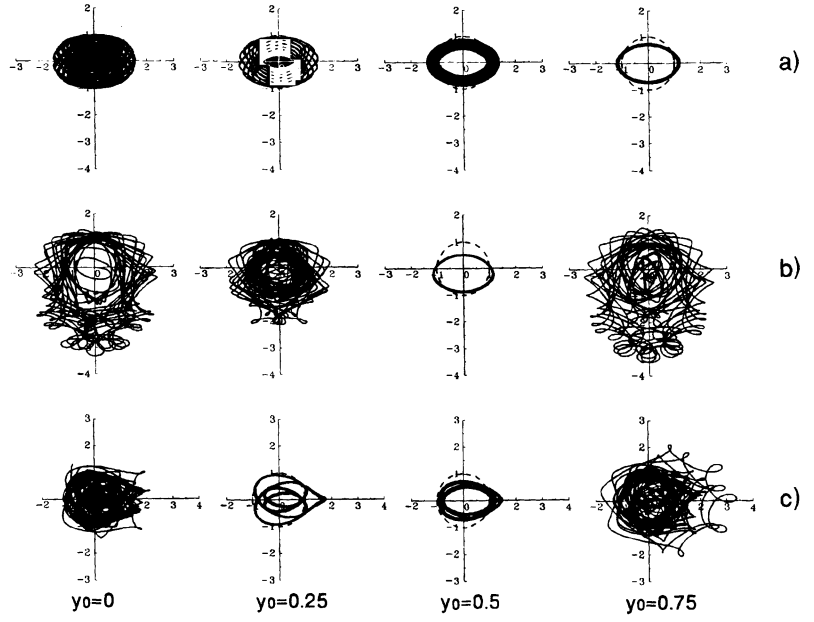

FIGURE 4 Trajectories of a fluid particle, calculated numerically for $\sigma = 3$, $\omega = 1.5$, $x_0 = O$, $U = 0.8$, $V = 0.5$ and $[U_0 : V_0]$ = (a) [0:0], (b) [0.25:0] and (c) [0:0.25], for y_0 values shown.

here with those observed in a rather different physical system by Boyer *et al.* (1991).

In Figures 5a and 5b, where the external parameters match the background field of Figure 1, plots are presented to confirm the suppositions (a)–(c) (see Section 2.1 above) on the existence of solutions that have been given in the previous section. Detailed examination of the class (c), the most substantial of the topological properties, has revealed some regularity in the transition from finite to infinite motions. Of course, the numerical calculation over the finite time interval can relate the solution to one of the named types only approximately. When determining the finite solutions, the calculations were carried out over the interval $[0, T]$, $T = 3000$. This exceeds by three orders of magnitude the range of characteristic time variation, indicating that $t \to T$ and $t \to \infty$ are practically equivalent for the present purposes. If the solution retains its quasi-periodic character over all this interval, it is adopted as belonging to the class of finite

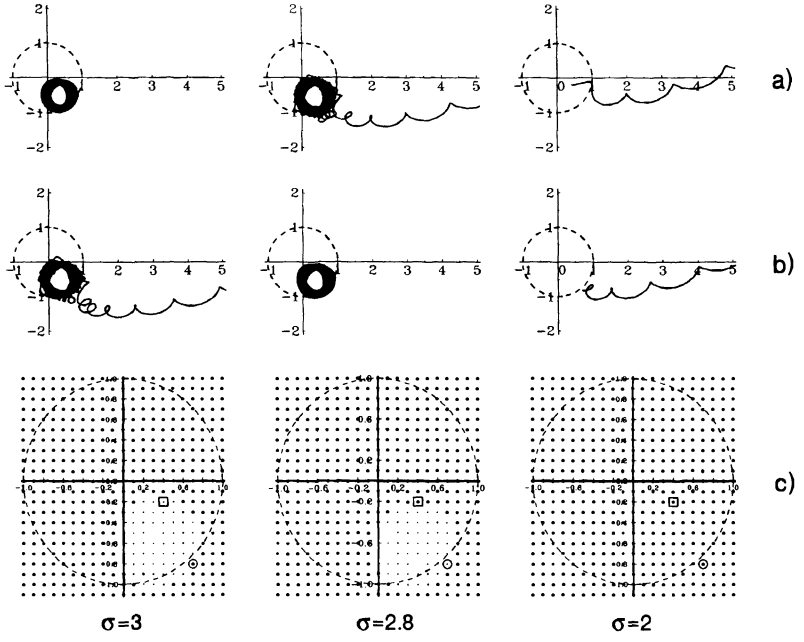

FIGURE 5 Trajectories (a, b) of a fluid particle at $\omega=\pi$, $U_0=0.75$, $V_0=0.5$, $U=0.6$, $V=0.5$ and $[x_0, y_0]$ values (a) [0.4: −0.2]; (b) [0.7: −0.8], together with (c) schematic map of distributions of finite and infinite solutions with respect to initial conditions (see text).

solutions for the given set of parameters. If this property is broken (*i.e.*, when a particle is no longer in the vicinity of the topographic feature and begins to move away quickly), the solution should clearly be regarded as infinite.

Figure 5 gives the results of calculations made according to such a scheme. Here, all points of the named area of the plane (x, y) are marked with the interval 0.1 in the sense of every variable. For all of these points taken as initial conditions (x_0, y_0) solutions were obtained by solving the Cauchy problem (6)–(8). Particles that have been advected from the vicinity of the topography and those that are trapped are shown in bold and normal styles respectively. The points marked with squares and circles correspond to the initial conditions of the problem, its solution being illustrated by Figures 5a and 5b respectively. It is important to note that the trapped category can include not only those particles that have been located initially over

the topography, but also those outside it. Four frames in the upper left corner of Figure 5 demonstrate a significant property of the flow, that, depending upon its initial position, the particle can be trapped by a shallow topography but can drift from a feature of greater height. Figure 6 shows the phenomenon of the alternation of domains of existence for finite and infinite solutions with respect to kinematic parameters of the external field. This phenomenon is a specific peculiarity, appearing due to the non-stationarity of the background field, whereas in the problem of topographic cyclogenesis in stationary flow over an isolated hill, the ratio between critical velocity values of the current and the hill height is uniquely determined (Kozlov, 1983; Zyryanov, 1985, 1995). This figure represents a map of the external parameter set; these parameters characterise both finite and infinite motion of the liquid particle in the background flow which has only non-zero steady state x-component. In Figure 6a the particle has initial coordinates (0, 0) and the tidal oscillations occur only in the x direction; in Figure 6b the initial position is (0, 0.5) and the tidal motion corresponds to circular rotation. Examples of the system (6)–(8) solutions, coordinated with Figure 6, are given in Figure 7, where transitions from finite to infinite motions (and *vice versa*) are

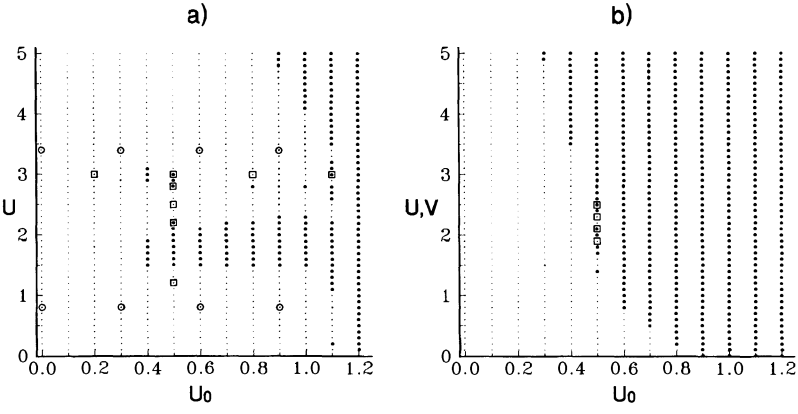

FIGURE 6 Distribution of domains of existence for finite (normal) and infinite (bold) solutions in the beginning of the first quadrant of the plane defined by constant component of the current amplitude of the tide, at $\omega=\pi$, $\sigma=4$, $x_0=0$, $V_0=0$ for (a) $y_0=0$, $V=0$; ~~(b) $y_0=0.5$, $V=0$ and~~ (b) $y_0=0.5$, $U=V$. Points are placed with intervals 0.1 in the directions of both coordinate axes. Square and circular symbols correspond to the points representing the experiments shown in Figures 7 and 9 respectively.

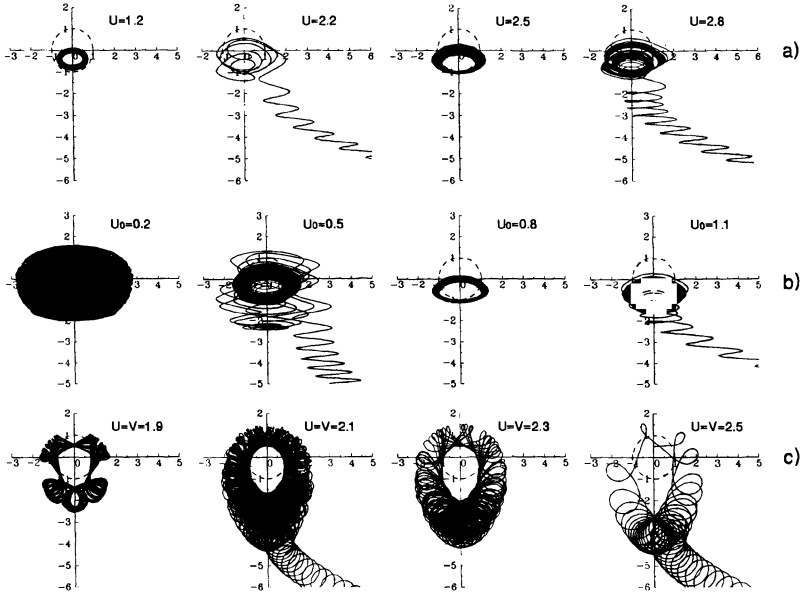

FIGURE 7 Trajectories of a fluid particle at $\omega=\pi$, $\sigma=4$, $x_0=0$, $V_0=0$ and (a) $y_0=0$, $U_0=0.5$, $V=0$; (b) $y_0=0$, $U=3$, $V=0$ and (c) $y_0=0.5$, $U_0=0.5$, $U=V$.

demonstrated as the different parameters increase monotonically. Note that points marked with squares on Figure 6 characterise the parameters at which these calculations have been made. One of the most interesting cases is demonstrated in Figure 7b, where the particular possibility of transition from separated to trapped flows when the drift component of the background flow increases is illustrated.

Sets of various finite trajectories are demonstrated in Figures 8 and 9. A non-zero steady state y-component of velocity is the characteristic feature of the external field in the series of experiments represented by Figure 8. In this case, $a=0$, $b=y_0$ and the parameters have been chosen such that $B/C\cong 0.4$. In this manner, if the particle stays over the obstacle during its motion it performs periodic rotation (See Figs. 8b and 8c) according to (25). It is clear that at $y_0=0.4$, the trajectories become elliptic when $D=0$. The evident similarity of figures that the particle performs at equal values of $|y_0-0.4|$ may be explained by the fact that, in these cases, the value of D in (25) has

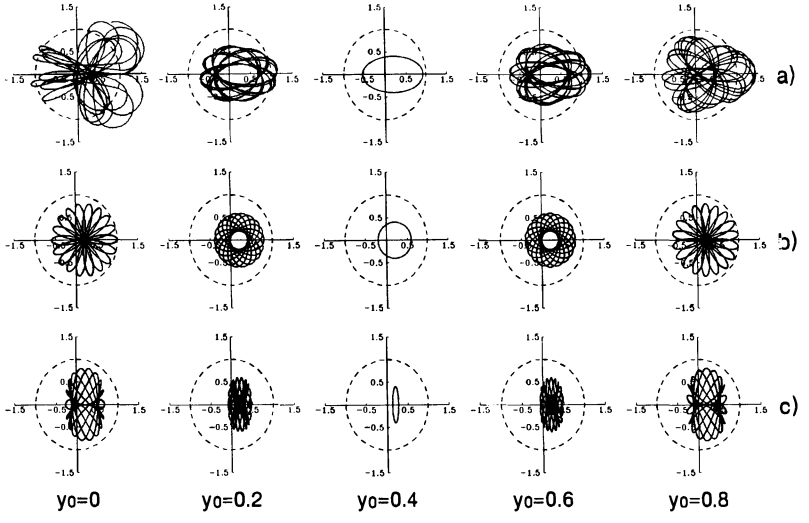

FIGURE 8 Trajectories of a fluid particle at $\omega=\pi$, $\sigma=4$, $x_0=0.2$, $U_0=0$, $V_0=0.4$ ($a=0$) and (a) $U=V=-2.057$; (b) $U=-3.085$, $V=-2.711$ and (c) $U=-1.028$, $V=-1.402$.

values equal in magnitude but opposite in sign. Figure 9 illustrates the influence of U and U_0 on the structures of the particle trajectories: the growth of the steady state x-component of the current results in a deviation to the right of the whole configuration and the increase of the amplitude of tidal oscillations along the x-axis causes a bigger deviation of the particle in both the x- and y-directions. Note that the configurations are symmetrical with respect to the axis normal to the background flow. As this model does not take friction into consideration, no phenomenon of tidal rectification (Perenne *et al.*, 1997) is observed here.

2.3. Dynamics of a Patch of Passive Admixture in the Vicinity of Bottom Topography

The discrete model discussed above may be used for a qualitative description of the motion of very small fluid volumes, but oceanic observations (Darnitskiy, 1980) show that the horizontal scale of anomalous concentrations of different mineral elements in topographically-controlled regions have, as a rule, dimensions of the order of

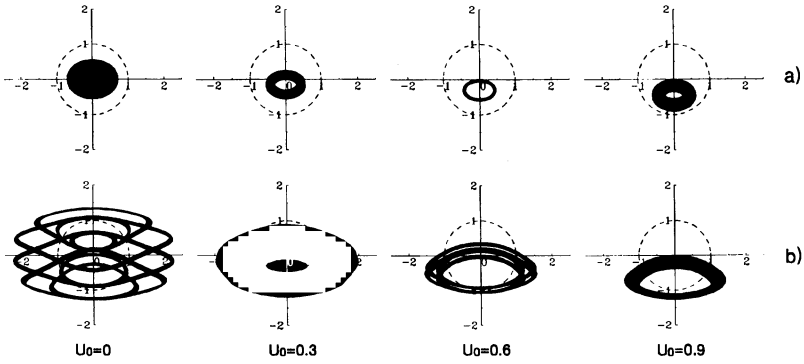

FIGURE 9 Trajectories of a fluid particle at $\omega=\pi$, $\sigma=4$, $x_0=0$, $y_0=0$, $v_0=0$, $V=0$ and $U=$(a) 0.8 and (b) 3.4.

the lateral size of the topographic features. In order to investigate the evolution of finite size admixture patches, it is possible, in particular, to follow the movement of points belonging to their conditional external boundaries. The Contour Dynamics Method appears to be the most convenient way of studying the dynamics of such boundaries, taking advantage, in the process, of the modification of an algorithm (Kozlov, 1983) based on a procedure using periodic cubic splines for numerical interpolation, differentiation and integration of network functions. Ordinary differential equations for the marker movement have been integrated by the Runge-Kutta method of the 4th order of accuracy through the use of "optimum" Gill formulae (Hairer *et al.*, 1987). The number of reference points was taken in such a way that along the unit radius circumference were 60 nodes.

The first series of numerical experiments, the results of which are plotted in Figure 10, had as its principal aim the comparison of modelling results for discrete and contour models. In the given background field, a fluid particle placed initially in the point (0, 0) moves along a circular orbit tangentially to both the abscissa axis in the point $x=0$ and the unit circumference in the point $(0, -1)$. Figure 10 demonstrates the evolution of the outer boundary of an admixture patch initially extending over the full area of the obstacle. As is apparent from the figure, the patches become deformed and then divide into parts, with one being advected by the flow and the other acquiring a relatively-compact form and remaining further inside

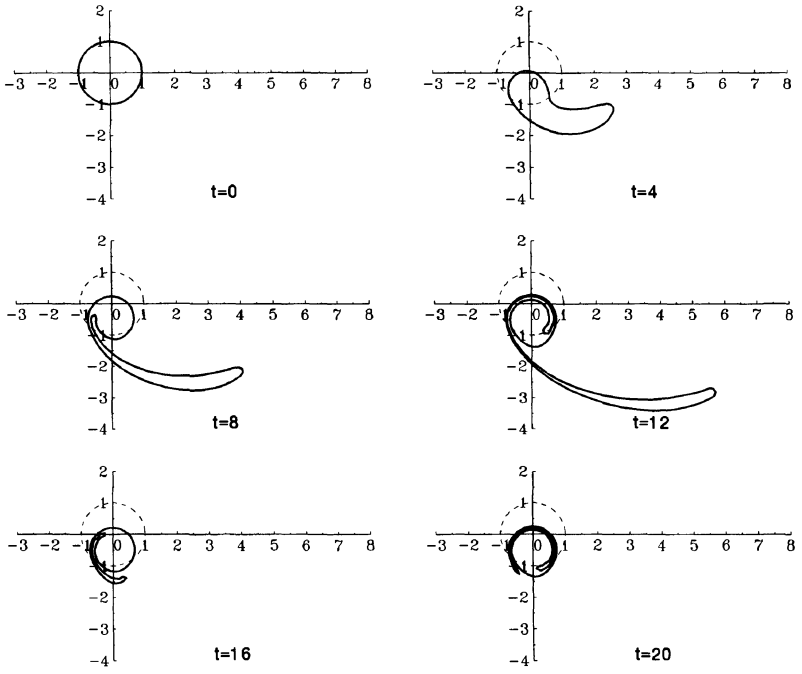

FIGURE 10 Calculation results for the patch of unit radius at $\omega=\pi$, $\sigma=2$, $U_0=0.5$, $V_0=U=V=0$.

the Taylor column boundary coincident with the trajectory of the standard fluid particle.

Figures 11a and 11b demonstrate the evolution of circular patches of unit radius for the same sets of external parameters as Figure 5 at $\sigma=3$ and $\sigma=2$. In the first case, the patch structure disintegrates; its significant mass is advected out of the vicinity of the obstacle while the portion that remains trapped by the topography performs quasi-periodic oscillations of small amplitude while remaining inside the area limited by the corresponding sepatratrix. Note that in the three upper rows of the figure, the patch contours are drawn using an interval of two units of dimensionless time (*i.e.*, 1 day) and in the lower row an interval of 0.5 is used to resolve and show changes during a tidal half period. In the second case (Fig. 11b), the patch is completely advected by the flow from the vicinity of the topography. Note that, according

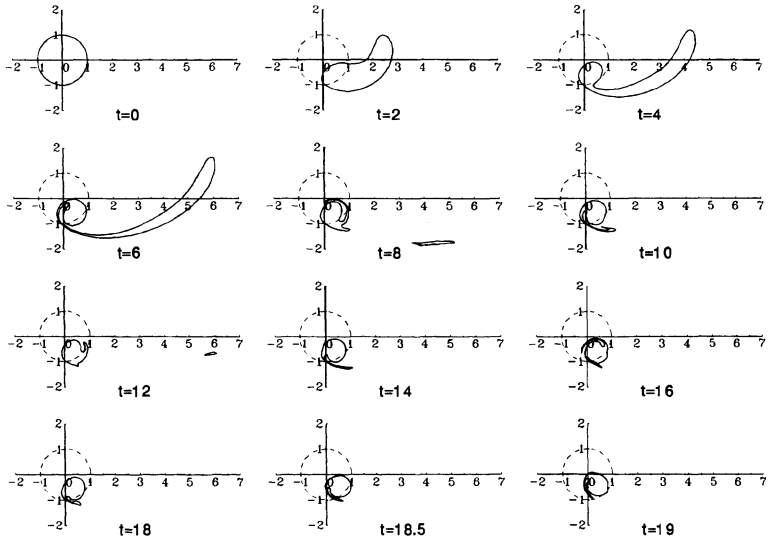

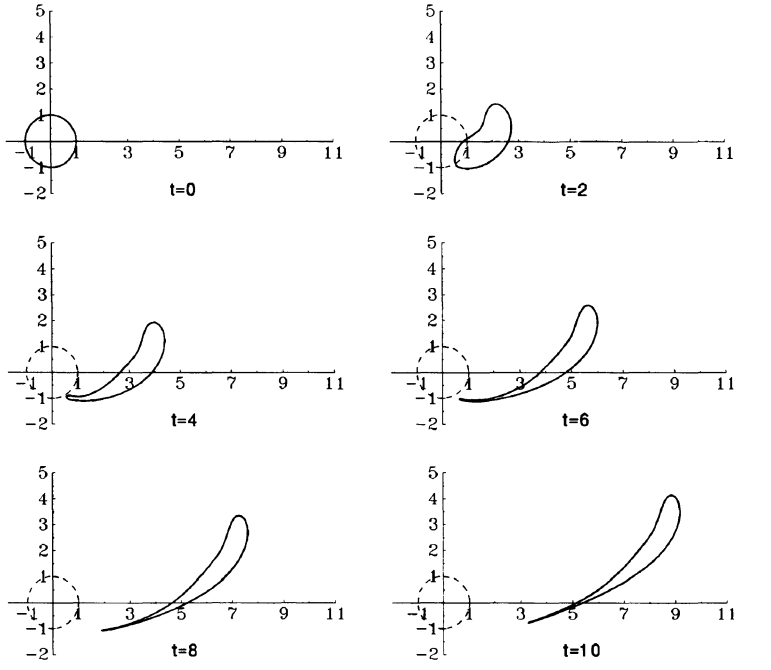

FIGURE 11 Evolution of initially-circular patches of unit radius at $\omega = \pi$, $U_0 = 0.75$, $V_0 = 0.5$, $U = 0.6$, $V = 0.5$ and $\sigma =$ (a) 3 and (b) 2.

to Figure 5c, there are no trapped portions of the patch in this region above the obstacle.

3. DIMENSIONAL VALUES OF MODEL PARAMETERS

All parameters cited in the text and the figure captions are given in dimensionless form. In Table I, relationships are presented between the values of the dimensionless parameters and their oceanic counterparts defined by the typical scales in Section 2. Note that the multiple values shown in the cells of the table relate directly to the corresponding values in the appropriate parts of figures. Initial coordinates of the point x_0, y_0 are given with respect to the centre of the submerged obstacle.

4. DISCUSSION OF RESULTS

The analytical and numerical calculations presented above provide information on the dynamics of flow over a bottom topographic feature – a flow that even in the simplest model of a barotropic tidal current is found to be complex. The dynamics of the flow have been studied from the point of view of Lagrangian particle movement, in order to identify with elements of passive admixture. It has been shown that it is possible to formulate the sufficient conditions for such a class of individual fluid particle motions when such particles stay always within the Taylor column defined by the imaginary upright cylinder circumscribing the (cylindrical) obstacle. In general, the particle performs rather intricate quasi-periodic oscillations. For specific (periodic) relationships between the height of the obstacle and the frequency of the tide, the oscillations are ellipsoidal or leaf-shaped. The relative ordering of some trajectories drawn in Figures 8 and 9 for particles located over the obstacle can be explained by the approximative fulfilment of the above relationships.

If the particle leaves the boundary of the obstacle, it can either (i) remain for a relatively long time in its vicinity, performing quasi-periodic oscillations (which are also sometimes quite ordered), or (ii) be advected downstream, depending on the relationship between the

TABLE I

Figure		*Non-dimensional parameters*							
		ω	σ	x_0	y_0	U_0	V_0	U	V
1	a) b) c)	3.14	3.0 2.8 2.0	–	–	0.75	0.50	0.60	0.50
2	a)	2;	4	0	0.0	0.00	0	2; 3; 4; 5	2; 3; 4; 5
	b)	4;			0.5	0.00	0	1; 1.5; 2; 2.5	1; 1.5; 2; 2.5
	c)	6;			0.5	0.00	0	0; 2; 2.66; 3.34	0; 1; 1.33; 1.67
	d)	8			0.5	0.25	0	0; 1; 1.34; 1.68	0; 0.5; 0.67; 0.84
3	a) b)	3.14	4; 0	0.108	−0.954	0.500; 0 0.182; 0	0.216; 0	0; 2.212 3.941; 2.212	0; 2.212 4.121; 2.713
4	a) b) c)	1.5	3	0	0; 0.25; 0.50; 0.75	0.00 0.25 0.00	0.00 0.00 0.25	0.8	0.5
5	a) b) c)	3.14	3; 2.8; 2	0.4 0.7 −1.0÷1.0	−0.2 −0.8 −1.1÷1.0	0.75	0.5	0.6	0.5
6	a) b)	3.14	4	0	0.0 0.5	0÷1.2	0	0÷5 0÷5	0 0÷5

	a)				0.0	0.5		1.2; 2.2; 2.5; 2.8	0
7	b)	3.14	4	0	0.0	0.2; 0.5; 0.8; 1.1	0	3	0
	c)				0.5	0.5		1.9; 2.1; 2.3; 2.5	1.9; 2.1; 2.3; 2.5
	a)				0; 0.2;			−3.085	−2.711
8	b)	3.14	4	0.2	0.4; 0.6; 0.8	0	0.4	−2.057	−2.057
	c)							−1.028	−1.402
9	a)	3.14	4	0	0	0; 0.3; 0.6; 0.9	0	0.8	0
	b)							3.4	
10		3.14	2	All points of the unit circle		0.5	0	0	0
	a)	3.14	3	All points of the unit circle		0.75	0.5	0.6	0.5
11	b)		2						
	a)	–	1.00;	–	–	–	–	–	–
12	b)	3.14	0.63; 3.36	0	0	0.3	0.15	1	0.5

TABLE I (Continued)

Figure		*Corresponding dimensional values*							
		$\omega^*(s^{-1})$ $\times 10^4$	$h(m)$	$x_0^*(m)$	$y_0^*(m)$	U_0^* (m/s)	V_0^* (m/s)	U (m/s)	V (m/s)
1	a) b) c)	1.45	1920 1792 1280		–	0.15	0.10	0.12	0.10
2	a)	0.92;			0	0.00	0	0.4; 0.6; 0.8; 1.0	0.4; 0.6; 0.8; 1.0
	b)	1.84;			2150	0.00	0	0.2; 0.3; 0.4; 0.5	0.2; 0.3; 0.4; 0.5
	c)	2.76;	2560	0	2150	0.00	0	0; 0.40; 0.53; 0.67;	0; 0.20; 0.27; 0.34;
	d)	3.68			2150	0.05	0	0; 0.20; 0.26; 0.34	0; 0.10; 0.13; 0.17
3	a) b)	1.45	2560; 0	464.4	−4102.2	0.100; 0 0.036; 0	0.043; 0	0; 0.442 0.788; 0.442	0; 0.442 0.824; 0.543
4	a) b) c)	0.69	1920	0	0; 1075 2150; 3225	0.00 0.05 0.00	0.00 0.00 0.05	0.16	0.10
5	a) b) c)	1.45	1920; 1792; 1280	1720 3010 −4300÷ 4300	−860 −3440 −4730÷ 4300	0.15	0.10	0.12	0.10
6	a) b)	1.45	2560	0	0 2150	0÷0.24	0	0÷1 0÷1	0 0÷1

	a)				0	0.10		0.24; 0.44; 0.50; 0.56	0
7	b)	1.45	2560	0	0	0.04; 0.10; 0.16; 0.22	0	0.60	0
	c)				2150	0.10		0.38; 0.42; 0.46; 0.50	0.38; 0.42; 0.46; 0.50
	a)				0; 860;			−0.617	−0.542
8	b)	1.45	2560	860	1720; 2580;	0	0.08	−0.411	−0.411
	c)				3440			−0.206	−0.280
9	a)	1.45	2560	0	0	0; 0.06; 0.12; 0.18	0	0.16	0
	b)							0.68	
10		1.45	1280	All points located at 4300 m from the center of the topographic feature		0.10	0	0	0
11	a)	1.45	1920	All points located at 4300 m from the center of the topographic feature		0.15	0.10	0.12	0.10
	b)		1280						
12	a)	–	640;	–	–	–	–	–	–
	b)	1.45	403.2; 2150.4	0	0	0.06	0.03	0.2	0.1

external parameters (*i.e.*, velocity components of the stationary flow, characteristics of the tidal ellipse of the background flow and the height of the bottom topography disturbance). Moreover, this dependence can be ambiguous, leading to the alternation of domains of existence for finite and infinite solutions in external parameter space. As has been noted above, the transition from one class of motion to the other occurs in the vicinity of the separatrices. It is known from the theory of Hamiltonian systems (Lichtenberg and Lieberman, 1982) that layers of stochasticity can arise along the separatrices. It seems that the afore-mentioned ambiguity is connected with the failure of regularity of the corresponding solution. In the present case, the system (6)–(8) is a non-autonomous Hamiltonian system and has one degree of freedom, but the Hamiltonian and the position of the separatrix depend explicitly on time. Analogous peculiarities take place, for example, in a dynamic system with two degrees of freedom, connected with the mapping of Ulam (Lichtenberg and Lieberman, 1982). Note that the non-autonomous system (6)–(8) is equivalent to the autonomous counterpart with two degrees of freedom.

Comparison between numerical experiments described in two last sections show that investigations of fluid particle dynamics give significant information on the character of motion of finite liquid volumes and not only information on the displacements of centres of gravity. Many features of solutions obtained for the fate of Lagrangian particle can be interpreted appropriately for descriptions of admixture patch movements.

Finally, it is noted that the theoretical results described above have relevance to topographically-controlled vortices in the ocean, with some evidence (Zyryanov, 1995) to indicate not only the accumulation of fish around the summits of seamount topography but also the apparent requirement for the existence of such a vortex to ensure the localisation of a closed fish population. From the biological point of view, such a population is evidently viable only if eggs and fry are not advected from the vicinity of the seamount. However, hydrological studies have shown that even when no topographic vortex is established over the seamount and no closed streamlines exist for a current simply passing over the obstruction, stable fish populations can still be found. The present work indicates how this apparent

paradox can be explained by appealing to the importance of the tidal oscillation component of the flow in realising the type (c) regime (see Section 2.1 above). Likewise, the present study showing quasi-periodic trajectories extending over large areas demonstrates that in oceanic regions with significant tidal oscillations how even a small volume of pollutant can have an adverse effect on a large area of the basin.

Acknowledgements

The work has been completed thanks to the generous financial support of INTAS (Project 94-3614) and the Russian Fund for Basic Studies (Projects 95-05-14972 and 96-05-66265). Drs. D. L. Boyer and J. Verron are thanked for constructive comments that contributed to improvements in the manuscript and Mrs. O. I. Yakovenko is thanked for her technical assistance. One of the authors (MAS) is particularly grateful to Professor V. F. Kozlov for discussions with him of the results of the calculations.

References

Baines, P. G., *Topographic Effects in Stratified Flows*, Cambridge University Press, Cambridge, UK (1993).

Beckmann, A. and Haidvogel, D. B., "Numerical simulation of flow around tall isolated seamount. Part I: Problem formulation and model accuracy," *J. Phys. Oceanog.* **23**(8), 1736–1753 (1993).

Beerens, S. P., Ridderinkhof, H. and Zimmerman, J. T. F., "An analytical study of chaotic stirring in tidal areas," *Chaos, Solitons and Fractals* **4**(6), 1011–1029 (1994).

Boyer, D. L., Chabert d'Hières, G., Didelle, H., Verron, J., Chen, R. R. and Tao, L., "Laboratory simulation of tidal rectification over seamounts: homogeneous model," *J. Phys. Oceanog.* **21**(10), 1559–1579 (1991).

Brink, K. H., "Tidal and lower frequency currents above Fieberling Guyot," *J. Geophys. Res.* (*Oceans*) **100**(C6), 10817–10832 (1995).

Chen, C. and Beardsley, R. C., "A numerical study of stratified tidal rectification over finite-amplitude banks. Part I: Symmetric Banks," *J. Phys. Oceanog.* **25**(9), 2090–2110 (1995).

Chen, C., Beardsley, R. C. and Limeburner, R., "A numerical study of stratified tidal rectification over finite-amplitude banks, Part II: Georges Bank," *J. Phys. Oceanog.* **25**(9), 2111–2128 (1995).

Darnitskiy, V. B., "Baroclinic and barotropic topographic vortices in the ocean," Voprosy okeanographii, Collection of works of FERSI, Issue **86**, 51–70 (In Russian) (1980).

Eriksen, C. C., "Observations of amplified flows atop a large seamount," *J. Geophys. Res.* (*Oceans*) **96**, 15227–15236 (1991).

Foreman, M. G. G., Baptista, A. M. and Walters, R. A., "Tidal model studies of particle trajectories around a shallow coastal bank," *Atmosphere-Ocean* **30**(1), 43–69 (1992).

Gibson, C. H., Nabatov, V. and Ozmidov, R., "Measurements of turbulence and fossil turbulence near Ampere seamounts," *Dyn. Atmos. Oceans* **19**, 175–204 (1994).

Hairer, E., Norsett, S. P. and Wanner, G., *Solving Ordinary Differential Equations; I. Non-Stiff Problems*. Springer-Verlag, Berlin (1987).

Ingersoll, A. P., "Inertial Taylor columns and Jupiter's Great Red Spot," *J. Atmos. Sci.* **28**(4), 744–752 (1969).

Kozlov, V. F., "Contour Dynamics Method in model problems on the topography cyclogenesis in the ocean," *Acad. Sci. USSR. Phys. Atmos. and Ocean* **19**(8), 845–854 (1983).

Kozlov, V. F., *Models of Topographic Eddies in Ocean*, Nauka, Moscow (In Russian) (1983).

Kozlov, V. F. and Sokolovskiy, M. A., "Meander of a barotropic zonal current crossing a bottom ridge (Periodic regime)," *Oceanology* **21**(6), 684–687 (English translation) (1981).

Lichtenberg, A. J. and Lieberman, M. A., *Regular and Stochastic Motion*, Springer-Verlag, Berlin (1982).

Monin, A. S., Ozmidov, R. V. and Paka, V. O., "On the mesostructure of flow around underwater hills," *Dokl. Acad. Sci. USSR* **308**(1), 192–196 (In Russian) (1989).

Perenne, N., Verron, J., Renouard, D., Boyer, D. L. and Zhang, X., "Rectified barotropic flow over a submarine canyon," *J. Phys. Oceanog.* **27**(9), 1863–1893 (1997).

Perera, M. J. A. M., Fernando, H. J. S. and Boyer, D. L., "Mixing induced by oscillatory stratified flow past a right-circular cylinder," *J. Fluid Mech.* **284**, 1–21 (1995).

Roden, G. I., "Effect of seamounts chains on circulation and thermohaline structure," in *Seamount, Islands and Atolls, Geophys. Monogr. Ser.* **43**, 335–354, American Geophysical Union, Washington DC, USA (1987).

Roden, G. I., "Mesoscale flow and thermohaline structure around Fieberling seamount," *J. Geophys. Res.* (*Oceans*) **96**(C9), 16653–16672 (1991).

Smith, K. L., Schwab, W. C., Nobble, M. and Demousti, C., "Physical, geological and biological studies on 4 Pacific seamounts. Introduction," *Deep Sea Res. A* **36**(12), 1785–1790 (1989).

Thompson, L., "Flow over finite isolated topography," Ph.D. Thesis, MIT/WHOI-91-05, USA (1990).

Verron, J., "Topographic eddies in temporally varying oceanic flows," *Geophys. Astrophys. Fluid. Dynam.* **35**, 257–276 (1986).

Zhang, X. and Boyer, D. L., "Laboratory study of rotating, stratified, oscillatory flow over a seamount," *J. Phys. Oceanog.* **23**(6), 1122–1141 (1993).

Ziemniak, E. M., Jung, C. and Tel, T., "Tracer dynamics in open hydrodynamical flow as chaotic scattering," *Physica D* **76**, 123–146 (1994).

Zyryanov, V. N., *The Theory of Stationary Oceanic Currents*, Hydrometeoizdat, Leningrad, USSR (In Russian) (1985).

Zyryanov, V. N., *Topographic Eddies in the Dynamics of Sea Currents*, Institute of Water Problems of the Russian Academy of Sciences, Moscow (In Russian) (1995).

APPENDIX

All results of the present work have been presented in the context of the obstacle form being an upright circular cylinder, *viz.*

$$h(r) = \begin{cases} 1, & r \leq r_1, \\ 0, & r > r_1, \end{cases} \tag{A1}$$

where $r_1 = 1$. In order to indicate qualitatively the general applicability of the results to other geometric shapes, two further examples (as normalised functions) are given below:

(a) a truncated cone, described by

$$h(r) = \begin{cases} 1, & r \leq r_1, \\ 1 - (r - r_1)/(r_2 - r_1), & r_1 < r \leq r_2, \\ 0, & r > r_2. \end{cases} \tag{A2}$$

For the example studied here, the values $r_1 = 1$ and $r_2 = 1.5$ have been chosen.

(b) a half wave of the cosine-squared function, described by

$$h(r) = \begin{cases} \cos^2(\pi r/2), & r \leq 1, \\ 0, & r > 1. \end{cases} \tag{A3}$$

In case (A2), the counterpart expression for (5) is

$$G(r) = \begin{cases} 1, & r \leq r_1, \\ 2[(r_2/2) - (r_1^3/6r^2) - (r/3)]/[r_2 - r_1], & r_1 < r \leq r_2, \\ (r_1^2 + r_1 r_2 + r_2^2)/3r^2, & r > r_2, \end{cases}$$

and for case (A3)

$$G(r) = \begin{cases} [(1/2) + (1/\pi r)(\sin \pi r) - (1/\pi r)^2 (1 - \cos \pi r)], & r \leq 1, \\ [1 - (4/\pi^2)]/2r^2, & r > 1, \end{cases}$$

where, clearly, $G(0) = 1$.

Figure 12 illustrates the behaviour of a fluid particle initially situated over the centres of each of these obstacles. The kinematic characteristics of the background flow are such that the x-component has a value that is twice that of its y-component, both for steady state velocities and for amplitudes of tidal oscillations. The topographic parameter σ has been derived in such a way that the volume of the

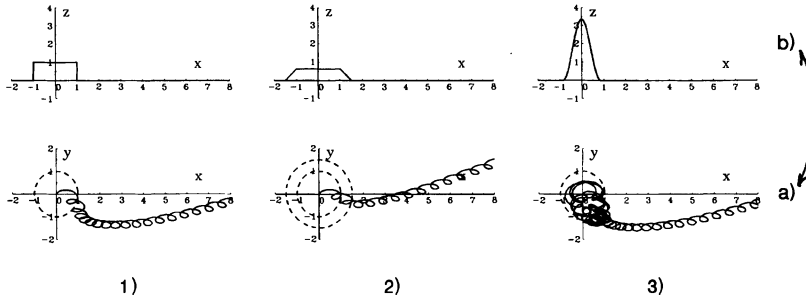

FIGURE 12 Vertical cuts of submerged obstacles (A1), (A2) and (A3) – (a) and trajectories of fluid particle motion at $\omega = \pi$, $x_0 = y_0 = 0$, $U_0 = 0.3$, $V_0 = 0.15$, $U = 1$, $V = 0.5$ and $\sigma = (1)\ 1$, (2) 0.63 and (3) 3.36 – (b).

bottom obstacle is the same in all three cases. The figure shows that though there is a clear qualitative similarity of trajectories, the "trapping" features of the obstacle (A3) are more pronounced.